Chapter 3

EFFECTS OF ANODIC POTENTIAL AND CHLORIDE ION ON OVERALL REACTIVITY IN ELECTROCHEMICAL REACTORS DESIGNED FOR SOLAR-POWERED WASTEWATER TREATMENT

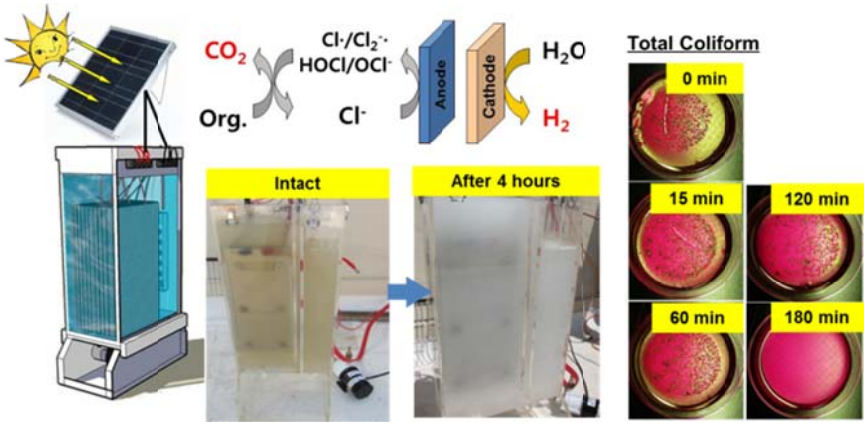

Sections reprinted with permission from Kangwoo Cho, Yan Qu, Daejung Kwon, Hao Zhang, Clement A. Cid, Asghar Aryanfar, and Michael R. Hoffmann *Environmental Science and Technology* **2014**, *48* (4), 2377-2384.

ABSTRACT

We have investigated the electrochemical treatment of real domestic wastewater coupled with the simultaneous production of molecular H_2 as a useful byproduct. The electrolysis cells employ multilayer semiconductor anodes with electroactive bismuth-doped TiO_2 functionalities and stainless steel cathodes. DC-powered laboratory-scale electrolysis experiments were performed under static anodic potentials (+2.2 or +3.0 V NHE) using domestic wastewater samples, with an added chloride ion in variable concentrations. Greater than 95% reductions in chemical oxygen demand (COD) and ammonium ion were achieved within 6 h. In addition, we experimentally determined a decreasing overall reactivity of reactive chlorine species toward COD with an increasing chloride ion concentration under chlorine radicals ($Cl\cdot$, $Cl_2^{-}\cdot$) generation at +3.0 V NHE. The current efficiency for COD removal was 12%, with the lowest specific energy consumption of 96 kWh $kgCOD^{-1}$ at the cell voltage near 4 V in 50 mM chloride. The current efficiency and energy efficiency for the H_2 generation were calculated to range from 34 to 84% and 14 to 26%, respectively. The hydrogen comprised 35 to 60% by volume of evolved gases. The efficacy of our electrolysis cell was further demonstrated by a 20 L prototype reactor totally powered by a photovoltaic (PV) panel, which was shown to eliminate COD and total coliform bacteria in less than 4 h of treatment.

3.1. INTRODUCTION

Sanitation in developing or emerging countries has been considered woefully inadequate, as illustrated by the fact that more than 1.8 million children under five years old die from waterborne diseases every year.[1] In developing countries, there is often a deficit of critical infrastructure, including electricity distribution grids and subsurface sewers that requires self-standing sanitation facilities for handling human waste. Given these circumstances, we describe and test a photovoltaic (PV) powered wastewater electrolysis cell (PWEC), which has been designed to couple the electrochemical treatment of wastewater with the production of molecular H_2 as a potentially useful byproduct. Application of modified PWEC may eventually lead to improved human sanitation in peri-urban regions, rural areas, or more remote locations that are currently lacking in conventional urban infrastructure and proper sanitation facilities.

In wastewater electrolysis cells (WEC), environmental pollutants can be eliminated either by the direct heterogeneous or indirect homogeneous oxidation pathway.[2] Surface-bound reactive oxygen species (ROS) are intermediates in O_2 evolution during water splitting, which may also result in the direct oxidation of chemical substrates.[3] ROS also reacts with chloride in wastewater to produce reactive chlorine species (RCS) such as free chlorine (Cl_2, HOCl, ClO^-) and chlorine radical species ($Cl\cdot$, $Cl_2^{-}\cdot$).[4,5] Organic substrates can be converted via reactions with RCS to CO_2 and an array of lower molecular weight carboxylic acids.[6] At the same time, with sufficient RCS generation, disinfection of fecal coliform bacteria can be achieved. Inexpensive polycrystalline photovoltaic (PV) panels can be used to convert incident solar irradiation into a direct

current (DC) potential across anode/cathode pairs to produce ROS.[7] Water oxidation at the anode is balanced in part by water/proton reduction at the cathode to produce H_2.

Electrochemical systems have often been investigated for treatment of model organic compounds or industrial wastewater using boron-doped diamond or mixed metal oxides electrode based on IrO_2 and RuO_2, mostly focusing only on anodic pollutants removal in DC-powered reactors.[3,4] In line with our previous reports[5-8] on the multifunctional approach of WEC with bismuth-doped TiO_2 anodes for wastewater treatment and molecular H_2 production, we first report the efficacy with real domestic wastewater by benchtop WEC and prototype PWEC experiments. While an existence of various reactive oxidants has been usually inferred based on the cell voltage,[5] this study employed potentiostatic electrolysis with monitoring of anodic/cathodic potential and ohmic loss. The experimental approach of this study provides more plausible explanations for the role of various oxidants in reference to their thermodynamic potentials.

3.2. EXPERIMENTAL SECTION

3.2.1. Electrode Module. The semiconductor anodes employed in this study were prepared according to a basic procedure described in our previous reports.[6,9] The procedure includes sequential thermal decomposition of mixed metal oxides including $Ir_{0.73}Ta_{0.27}O_x$, $Sn_{0.9}Bi_{0.1}O_x$, $Ti_{0.96}Bi_{0.04}O_x$, and $Ti_{0.66}Bi_{0.33}O_x$ on conductive Ti metal plates. An electron probe microanalysis[10] indicates that the outer surface of the synthesized electrodes is composed mainly of bismuth, titanium, and oxygen (BiO_x/TiO_2). The underlying layers involving the oxides of Ir, Ta, and Sn are reported to enhance the

stability and conductivity of the electrode.[9] The electrode module used for laboratory experiments consists of the BiO_x/TiO_2 anode (2.7 cm × 2 cm), stainless steel (SS) cathode (Hastelloy C-22, 2.7 cm × 2 cm), and Ag/AgCl/Sat. KCl reference electrode (BaSi Inc., USA). The distance between anode and cathode was 5 mm, while the frit tip of the reference electrode was located 2 mm apart from the center of the anode.

3.2.2. Characterization of the BiO_x/TiO_2 Anode. Cyclic voltammetry (CV) profiles were collected over a range of 0 to 2.0 V NHE by three repetitive scans (5 mV sec^{-1}) in quiescent 30 mM NaCl solution. In benchtop reactors, the electrode module was installed in a single compartment cell with working volume of 60 mL. A potentiostat (Bio-Logic, France) was used for controlling applied anodic potential (E_a) versus reference electrode, monitoring the response current (I) and the cathodic potential (E_c) versus reference electrode.

3.2.3. DC Powered Wastewater Electrolysis. Potentiostatic WEC experiments using domestic wastewater were performed under variable E_a and added electrolyte (NaCl) concentrations. The applied anodic potentials, E_a, were fixed either at 2.2 or 3.0 V NHE versus the reference electrode. The ohmic resistance between anode and reference electrode (R) was measured by current interruption method[11] with current bias of 200 mA, to estimate actual anodic potential ($E_a - iR$). Residential-strength wastewater samples were collected from the effluent line of a primary settling tank at the San Jose Creek Wastewater Treatment Plant (Whittier, CA, USA). The wastewater samples were stored at 4 ºC, and the supernatant after settling was used. The composition of the intact wastewater is given in Table 3.1. In rural areas, wastewater salinity and chloride

Table 3.1. Composition of residential-strength wastewater used in this study.

Constituent	Mean	COV (%)
pH	6.6 – 7.3	–
COD (mg L^{-1})	180	6.02
TN (mM N)	2.594	7.96
NH_4^+ (mM)	1.910	5.19
NO_3^- (mM)	< 0.01	–
Cl^- (mM)	3.880	–
ClO_3^- (mM)	< 0.01	–
Mg^{2+} (mM)	0.6387	1.96
Ca^{2+} (mM)	1.287	1.38

COV: Coefficient of Variation.

concentrations are normally higher than in urban areas.[12] Therefore, moderate amounts of NaCl were added with the added chloride concentrations ($[Cl^-]_{ext.}$) ranging from 0 to 50 mM. During the wastewater electrolysis, the wastewater electrolyte was stirred at 600 rpm by a magnetic bar (0.8 cm diameter × 1.8 cm). Over reaction durations of 200 to 230 min, gaseous products were collected in a graduated buret to determine average volumetric flow rates. The volumetric H_2 fraction in the collected gas was determined by a GC-TCD (Hewlett-Packard, USA), using a 5 V/V% H_2 standard gas for calibration.

3.2.4. Prototype PV Powered Wastewater Electrolysis. A 20 L WEC powered by a PV panel was tested in roof-top experiments in order to assess the feasibility of PV panels as the sole source of energy for COD elimination and disinfection due to *in situ* RCS generation. The PWEC system had an anode/cathode array module consisting of five doubly coated BiO_x/TiO_2 anodes and six SS cathodes (40 × 20 cm^2 each) with a distance of separation between each anode and cathode pair of 0.2 cm. A commercially available,

low-cost polycrystalline PV panel (Silicon Solar Inc., USA) was employed. More details are described in the Supporting Information. Twenty liters of wastewater with added NaCl of 50 mM was mixed with a circulation pump connected to the bottom of the reactor at the rate of 25 L min^{-1}. The $E_a - E_c$, and the current were periodically monitored using multimeters (Fluke, USA).

3.2.5. Analysis. COD and total nitrogen (TN) concentration of samples were measured based on the absorbance at 420 nm in UV-vis spectrophotometer (Agilent, USA), after digestion in a low-range dichromate digestion solution (3 – 150 mg L^{-1}, Hach, USA) and in a low-range TN reagent set (0.5 – 25 mgN L^{-1}, Hach, USA), respectively. Anions (Cl^-, ClO_3^-, NO_3^-,) and cations (NH_4^+, Ca^{2+}, Mg^{2+}) were simultaneously determined by ion chromatography (Dionex, USA), using anion-exchange column (Ionpac AS 19) and cation-exchange column (Ionpac CS 16). The total chlorine (Cl_{DPD}) was measured using DPD (N,N-diethyl-p-phenylenediamine) reagent (Hach, USA) coupled with quantification via absorbance measurements at 530 nm. A standard wastewater membrane filtration method was used to count the number of total coliforms and fecal coliforms during electrolysis (details in the Supporting Information).

3.3. RESULTS AND DISCUSSION

3.3.1. Characteristics of the BiO_x/TiO_2 Anodes. Figure 3.1 shows CV plots for the BiO_x/TiO_2 anode in a 30 mM NaCl electrolyte solution. The onset potential, which corresponds to 1 A m^{-2} of current density, initially appeared at near 1.2 V. In comparison to the reduction potential of O_2/H_2O couple at pH 7 (Table 3.2), the observed onset potential estimated oxygen evolution overpotential of 0.38 V. This value is quite

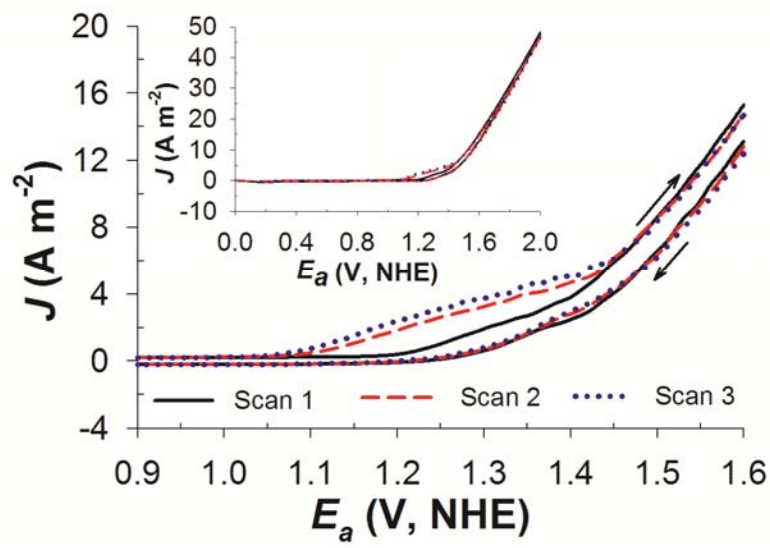

Figure 3.1. Cyclic voltammetry of the BiO_x/TiO_2 anode in 30 mM NaCl solution with three repetitive scans at a scan rate of 5 mV sec^{-1}. The full scans from 0 to 2 V NHE are shown in the inset figure.

Table 3.2. Reduction potential (E) at pH 7 and standard reduction potential (E^0) at pH 0 for several redox couples involved in the electrochemical reactions.

Redox Couple	at pH 7 (V NHE)	at pH 0 (V NHE)
O_2/H_2O	0.82	
Cl_2/Cl^-	1.36	1.36
$HOCl/Cl^-$		1.48
ClO^-/Cl^-		0.81
$Cl\cdot/Cl^-$		2.4
$Cl_2^-\cdot/Cl^-$		2.0
ClO_3^-/Cl_2	0.97	
$ClO_3^-/HOCl$	0.92	
ClO_3^-/ClO^-	0.94	

comparable to RuO_2 and IrO_2 based electrodes,[13] demonstrating that the BiO_x/TiO_2 electrode can be regarded as an active electrode for oxygen evolution. The activity may be attributed to intrinsic oxide vacancies of Bi_2O_3 in the lattice structure, which can facilitate the transition of surface-bound hydroxyl radicals to higher oxides.[14] Although a chloride oxidation peak is hidden by the large anodic wave from the oxygen evolution, chloride oxidation is generally accepted to produce Cl_2.[15,16] The Cl_2 will be in equilibrium with HOCl and ClO^- in bulk aqueous phase depending on the specific pH.[17] On the other hand, the second and third scan showed a significant decrease of the onset potential to 1.05 V, which would result from a formation of chlorate.[6] The ClO_3^- is known to be produced electrochemically either by oxidation of chloride or free chlorine (HOCl or ClO^-).[18,19] The decrease in onset potential in Figure 3.1 suggests that the chlorate is produced by the oxidation of the RCS[20] which requires four electrons for free chlorine oxidation.

As shown in Table 3.3, the current and ohmic drop between electrodes increases along with the chloride concentration and applied potential. As a result, actual anodic potential ($E_a - iR$) with 50 mM of chloride (H50) was smaller than those with lower added chloride (H10 and H30), while marginally higher than at lower E_a (L30 and L50). Another important observation was that a substantial cathodic potential is required to maintain the E_a; *i.e.*, the $E_a - E_c$ approaches about twice of the E_a. Consequently, the power consumption grows as the E_a or $[Cl^-]_{ext.}$ increases under the potentiostatic conditions.

Table 3.3. The *iR*-compensated anodic potential ($E_a - iR$), cell voltage ($E_a - E_c$), current density (J), and power consumption (P) on average under variable applied anodic potential (E_a; L: 2.2 V, H: 3.0 V NHE) and added Cl^- concentration ($[Cl^-]_{ext.}$; 0, 10, 30, 50 mM) in electrolysis experiments using domestic wastewater samples.

ID	$[Cl^-]_{ext.}$ (mM)	E_a (V NHE)	$E_a - iR$ (V NHE)	$E_a - E_c$ (V)	J (A m^{-2})	P (W)
L30	30	2.2	1.92 (2.8)	4.03 (0.94)	74.2 (19)	0.161 (20)
L50	50	2.2	1.96 (2.0)	3.88 (0.94)	89.4 (17)	0.188 (18)
H0	0	3.0	2.08 (5.8)	6.27 (1.2)	80.9 (13)	0.274 (14)
H10	10	3.0	2.24 (4.9)	5.56 (0.72)	110 (14)	0.367 (15)
H30	30	3.0	2.25 (4.8)	5.88 (0.72)	206 (14)	0.655 (15)
H50	50	3.0	2.00 (4.5)	5.37 (0.17)	296 (9.1)	0.953 (9.2)

Values in parentheses show coefficient of variation (%).

Figure 3.2 illustrates the current density as a function of $[Cl^-]$ during the wastewater electrolysis. At a given E_a and $[Cl^-]_{ext}$, the J was almost proportional to the $[Cl^-]$. Provided that the generation of RCS and oxygen accounts for the anodic electron transfer, it can be inferred that the rate of RCS generation is first-order in $[Cl^-]$, as reported previously for chlorine generation on RuO_2 anodes.[15,16] The apparent first-order kinetic on $[Cl^-]$ may also be a consequence of mass transport limitation. In addition, the rate of oxygen evolution can be also influenced by $[Cl^-]$. A decrease in $[Cl^-]$ should result in a decrease in the electrolyte conductivity and exchange current density for oxygen evolution.

3.3.2. Impact of E_a and $[Cl^-]_{ext.}$ on COD Removal. Figure 3.3 illustrates the effects of E_a on COD degradation under $[Cl^-]_{ext.}$ fixed either at 30 mM or 50 mM. Wastewater

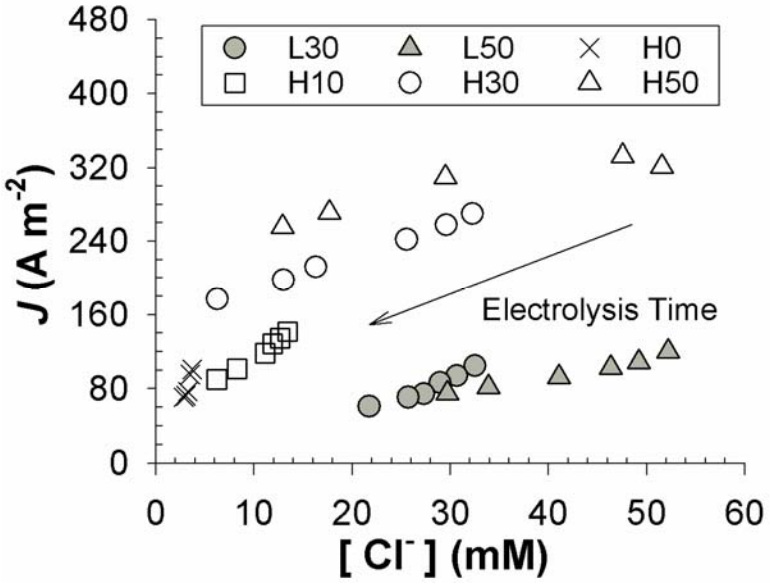

Figure 3.2. Evolution of current densities along with variations in Cl^- concentration under variable applied anodic potential (L: 2.2 V, H: 3.0 V NHE) and added Cl^- concentration (0, 10, 30, 50 mM) in electrolysis experiments using domestic wastewater samples. The arrow indicates an arbitrary varying direction as a function of time.

samples often contain refractory organics that are not detected as COD initially. The recalcitrant substrates are over time transformed by reactions with RCS to yield intermediate products that are more susceptible to the dichromate digestion, as indicated by a slight initial increase of COD.[21,22] When the COD concentration profiles were fit to pseudo-first-order kinetics, the rate constant increased with an increase in E_a. These results are consistent with COD removal in the low E_a that is limited by anodic electron transfer (heterogeneous RCS generation). Under the electron-transfer-limited regime, increasing cell voltage or the current density normally enhances the rate of pollutant degradation, except for those interfacial reactions that are controlled by mass transport.[13,20,22,23]

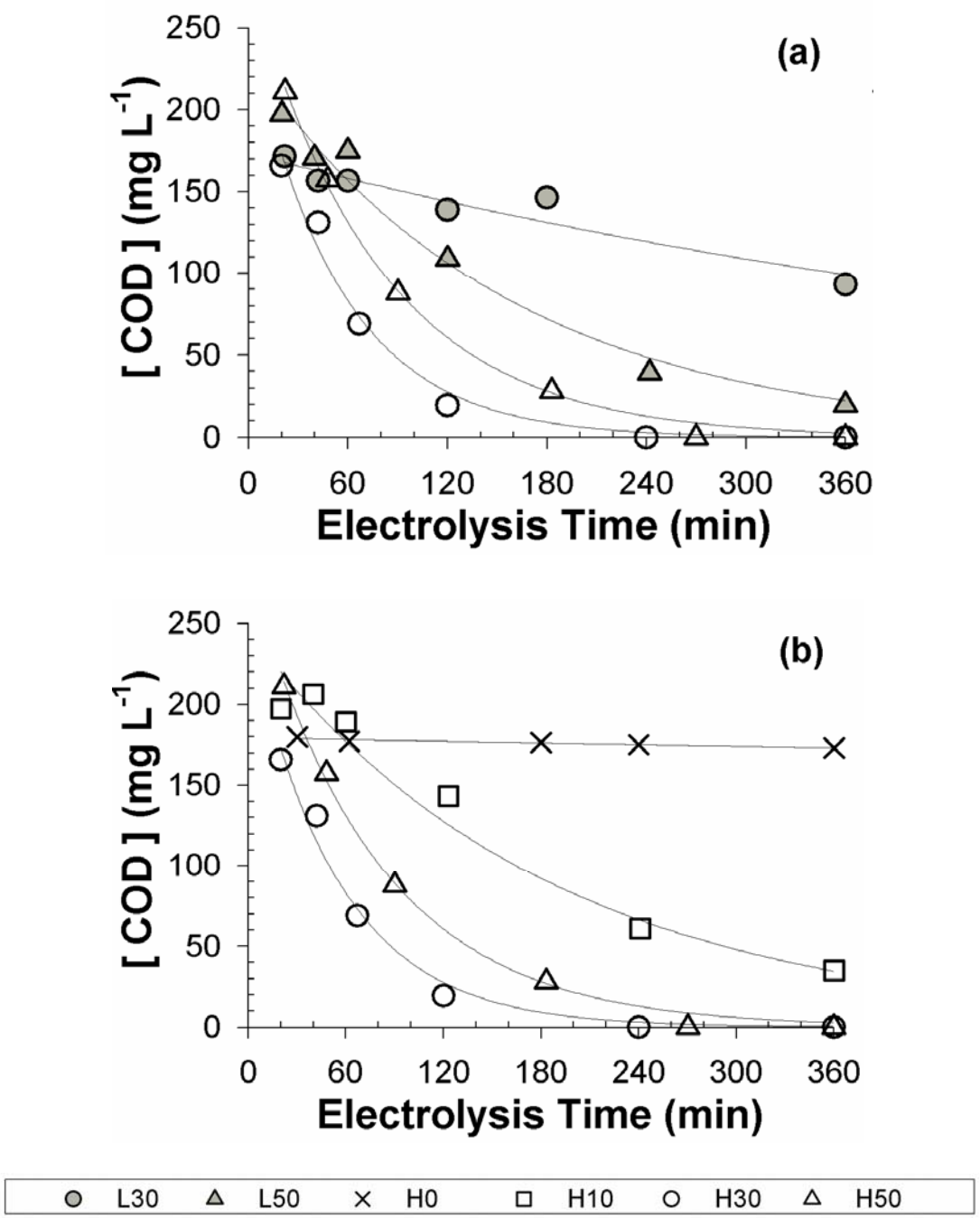

Figure 3.3. Time profiles of COD concentration under variable applied anodic potential (L: 2.2 V, H: 3.0 V NHE) and added Cl^- concentration (0, 10, 30, 50 mM) in electrolysis experiments using domestic wastewater samples. Time profile for each condition is regressed with a pseudo-first-order kinetic equation.

The effects of $[Cl^-]_{ext.}$ on COD removal at the high E_a (3.0 V NHE) are shown in Figure 3.3b. In this case, COD removal was not observed without the Cl^-, which indicates that direct oxidation via surface-bound hydroxyl radicals is a minor pathway on the BiO_x/TiO_2 electrode, as in the case of the RuO_x/TiO_2 electrode.[23-25] In contrast, elimination of measurable COD took less than 6 h with $[Cl^-]_{ext.}$ exceeding 10 mM. The pseudo-first-order rate constant for COD removal increased with increasing $[Cl^-]_{ext.}$ in the range of 10 mM to 30 mM, while a decrease in the rate of COD consumption was observed in the range of $[Cl^-]_{ext.}$ from 30 mM to 50 mM, even though there was an increase in J (Table 3.3). As a consequence, the net current efficiency (CE) for COD oxidation in H50 was smaller than in H10. This observation is contrary to some reports that increasing $[Cl^-]$ always enhances the rate and CE of COD removal[25-27] by increasing the overall rate of oxidants generation.[28] However, other studies report observed negligible[13,24,29] or adverse effects of $[Cl^-]$ in the range exceeding 30 mM, which were ascribed to pH decrease in the vicinity of the anode with increasing current density. The shift in the local pH may effectively shift the RCS speciation toward gaseous chlorine,[17] which results in a net loss of RCS. In this study, however, the bulk pH slightly increased from circum-neutral to ~9 in maximum along with the electrolysis. Therefore, we argue that there is a change in the speciation of RCS versus $[Cl^-]_{ext.}$ with corresponding shifts in the relative reactivity toward COD oxidation, which was not explained by the pH effects.

3.3.3. Impact of Cl· and Cl_2^-· on COD Removal. The effects of $[Cl^-]_{ext.}$ were interpreted using a simple kinetic model applied to the data of experiments H10, H30, and H50. The CV profiles (Figure 3.1) suggested that the oxidation of Cl^- produces RCS and chlorate in series. The oxidation of Cl^- and RCS as well as the homogeneous reaction

between the RCS and COD were assumed to be first order in each reactant.[19,24,27] The linear dependence of J on the [Cl^-] (Figure 3.2) is consistent with first-order kinetics for RCS generation as follows:

$$\frac{d[RCS]}{dt} = k_1[Cl^-] - k_2[RCS]_{SS}[COD] - k_3[RCS]_{SS} \approx 0 \quad (3.1)$$

$$\frac{d[COD]}{dt} = -k_2[RCS]_{SS}[COD] \approx -k_{COD}[COD] \quad (3.2)$$

$$\frac{d[ClO_3^-]}{dt} = k_3[RCS]_{SS} \approx k_{ClO_3^-} \quad (3.3)$$

$$k_2 = k_3 \frac{k_{COD}}{k_{ClO_3^-}} \quad (3.4)$$

where, k_1, k_2, and k_3 are rate constant for heterogeneous Cl^- oxidation to RCS, homogeneous reaction between RCS and COD, and heterogeneous RCS oxidation to chlorate. In addition, we assume a pseudo-steady-state condition for the rate of RCS production. The total chlorine concentration was negligible when the COD concentration was higher than 100 mg L^{-1} (Figure 3.4a). A linear relationship between [Cl^-] and [COD], indicated by eq 3.1 with quasi-constant [RCS], is supported by Figure 3.4b. Furthermore, the steady-state assumption for [RCS] is self-consistent with the decrease in [COD] versus time, which follows apparent pseudo-first-order kinetics (Figure 3.3). Therefore, the pseudo-first-order rate constant for COD removal (k_{COD}) and the pseudo-zero-order rate constant for chlorate production ($k_{ClO_3^-}$) can be expressed as the steady-state RCS concentration ($[RCS]_{SS}$) multiplied by the reactivity of the RCS toward the COD (k_2)

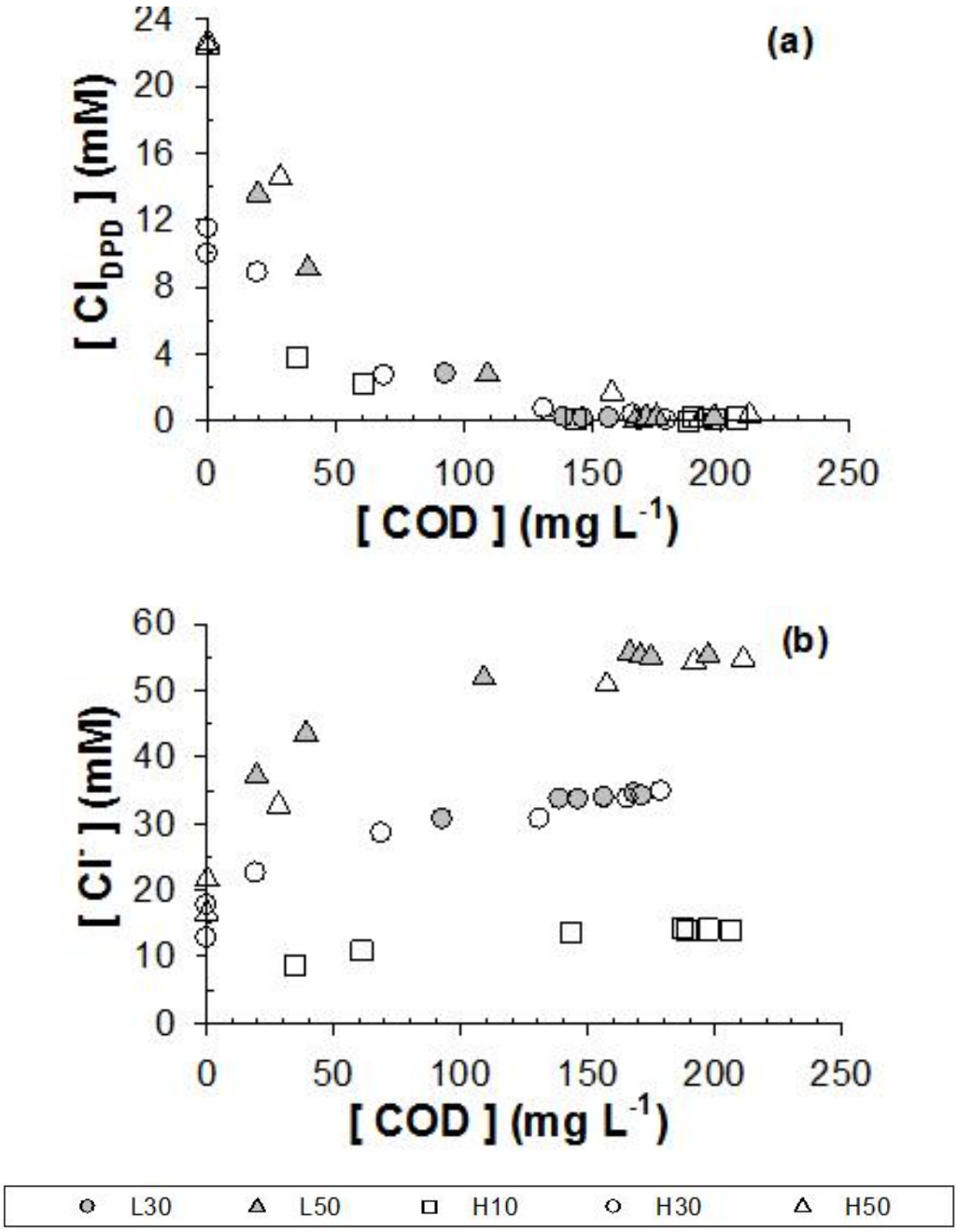

Figure 3.4. Evolutions of (a) total chlorine (Cl_{DPD}) and (b) Cl^- concentration as functions of variations in COD concentration under variable applied anodic potential (L: 2.2 V, H: 3.0 V NHE) and added Cl^- concentration (10, 30, 50 mM) in electrolysis experiments using domestic wastewater samples.

and heterogeneous rate constant (k_3), respectively. It could be argued that the heterogeneous rate constants, k_1 and k_3, should vary with the electrolysis time as given by the Butler-Volmer formulation.[11] However, relatively low variations in $E_a - iR$ (Table 3.3) are consistent with the assumption that k_1 and k_3 are essentially constant. Our recent report[6] demonstrated that the chloride oxidation kinetics are governed by consistent parameters regardless of initial chloride concentration during potentiostatic (E_a: 3 V NHE) electrolyses in NaCl solutions. The heterogeneous reactions on the metal oxide semiconductors are often controlled by rate constants between surface ROS and substrates that are independent of anodic potential.[2]

Figure 3.5 shows [ClO_3^-] increasing faster after depletion of [COD]. Nevertheless, the rate of ClO_3^- formation appeared almost constant when the steady-state assumption for [RCS] was valid, as shown in Figure 3.5 (inset). From the observed $k_{ClO_3^-}$ and k_{COD}, the k_2 / k_3 was calculated to be 1.1 mM^{-1} for H10, 0.60 mM^{-1} for H30, and 0.31 mM^{-1} for H50. Assuming that the k_3 is similar in each case, the reactivity between the RCS and COD (k_2) decreases as the $[Cl^-]_{ext.}$ increases. As shown in Table 3.3, the $E_a - iR$ values for H10 and H30 are sufficient to produce $Cl_2^-\cdot$, a stronger oxidant than free chlorine (Table 3.2). The $E_a - iR$ for H50 is close to the edge of the redox potential required for radical generation and lower than for H10 and H30 due to a higher solution resistance. Furthermore, $Cl_2^-\cdot$ is in equilibrium with Cl·, which has a redox potential higher than $Cl_2^-\cdot$.[5] Thus, under chlorine radicals generation, increasing [Cl^-] favors the formation of $Cl_2^-\cdot$ to Cl·, resulting in a net lower reactivity in terms of the rate of COD oxidation.

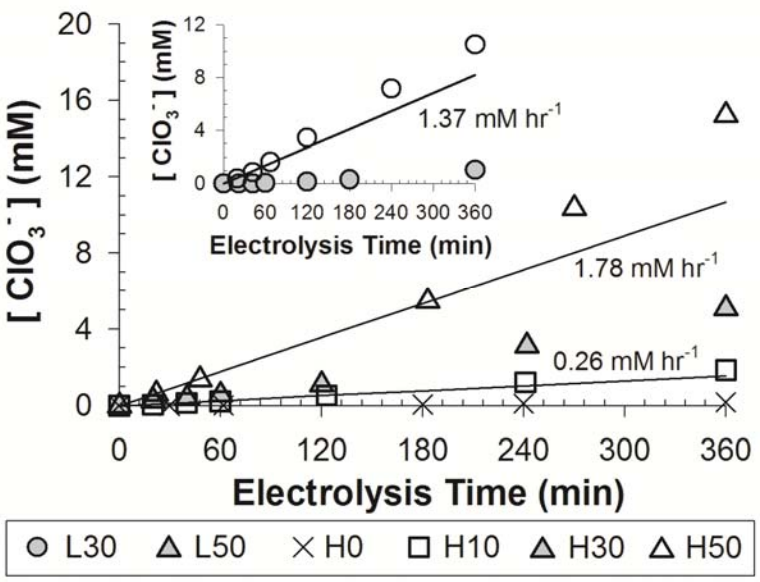

Figure 3.5. Time profiles of ClO_3^- concentration in electrolysis experiments using domestic wastewater samples under variable applied anodic potential (L: 2.2 V, H: 3.0 V NHE) and added Cl^- concentration (0, 10, 30, 50 mM). For H10, H30, and H50, regression lines for linearly increasing regions (initial 4 data points) are shown with corresponding zero-order rate constants.

3.3.4. Nitrogen Species. In the wastewater samples, the sum of $[NH_4^+]$ and $[NO_3^-]$ constituted more than 95% of [TN]. As shown in Figure 3.6a, $[NH_4^+]$ decreased to near zero within 3 h of electrolysis, except in the absence of added Cl^- (Figure 3.6a). The pseudo-first-order rate constants for NH_4^+ loss were higher than those for COD removal. A more facile oxidation of NH_4^+ than for various organic compounds (*i.e.*, COD) has also been reported for tannery wastewater[30] and landfill leachates.[28] The reaction rates of RCS generated at anode surfaces toward NH_4^+ and COD are often affected by mass transport.[31] Results show that NO_3^- increases with time but not in a normal stoichiometric relationship (Figure 3.6b). This is due to a substantial fraction of NH_4^+ that is converted to N_2. The sequential chlorination of NH_4^+ is known to produce the N_2 via breakpoint

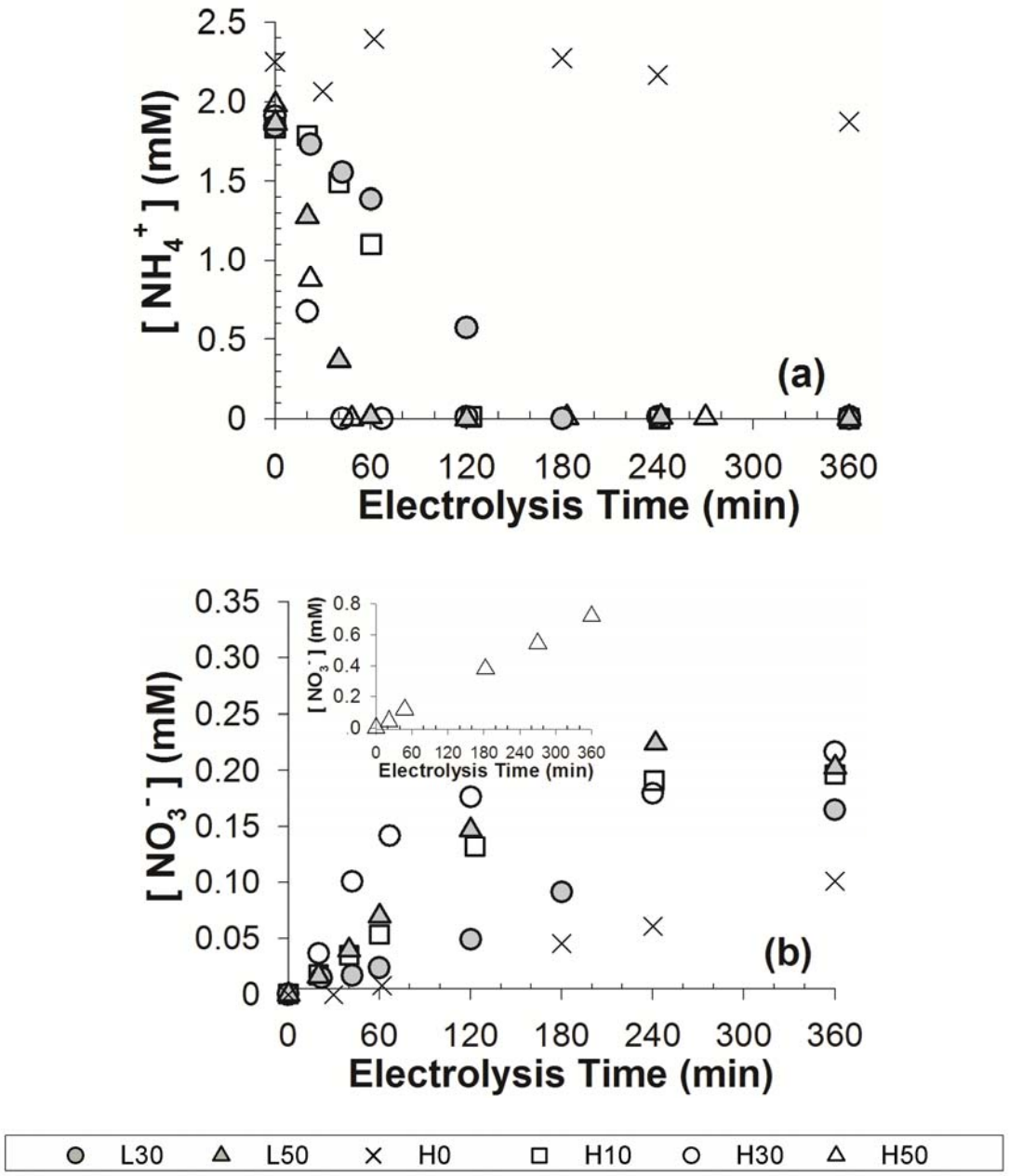

Figure 3.6. Time profiles of (a) NH_4^+ and (b) NO_3^- concentration under variable applied anodic potential (L: 2.2 V, H: 3.0 V NHE) and added Cl^- concentration (0, 10, 30, 50 mM) in electrolysis experiments using domestic wastewater samples.

chlorination.[17,28,32] For landfill leachates,[33] N_2 formation rate exceeded that of NO_3^-, especially as current densities or [Cl^-] increased.

3.3.5. CE and Energy Consumption for Anodic Reactions. The efficiency of electrochemical reactions is often expressed in terms of current efficiency, CE.[3,4] Figure 3.7 shows the general CE (eq 3.5) for the anodic reactions in the various wastewater electrolyses.

$$\text{Current Efficiency (CE) for Anodic Reaction } i\ (\%) = \frac{n_i \times F \times \left| C_i^{\,0} - C_i^{\,t} \right| \times V}{\int_0^t I dt} \times 100 \qquad (3.5)$$

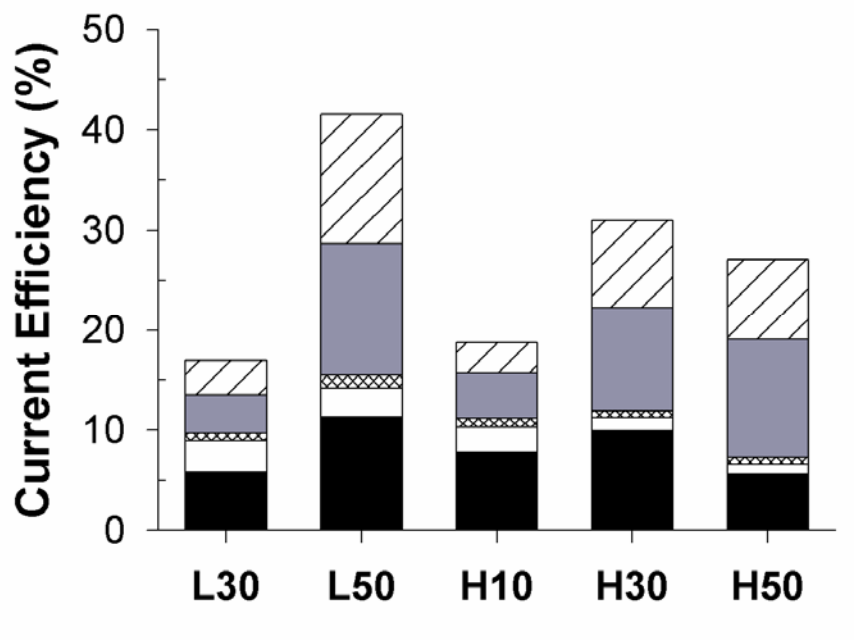

Figure 3.7. General current efficiencies for anodic reactions including COD oxidation (▬), formation of N_2 (▭), NO_3^- (▩), ClO_3^- (▬), and free chlorine (▨) under variable applied anodic potential (L: 2.2 V, H: 3.0 V NHE) and added Cl^- concentration (10, 30, 50 mM) in electrolysis experiments using domestic wastewater samples. Estimates are based on the time when COD decreases to below 30 mg L^{-1}.

where, C_i^0 and C_i^t are the concentration of species *i* (M) at the electrolysis time of zero and *t* (s), *V* is the volume of the electrolyte (0.06 L), *I* is the current (A), *F* is Faraday constant (96485.3 C mol^{-1}), and n_i is the number of electrons required to oxidize one mole of species *i*; 4 for oxidation of COD expressed in $molO_2\ L^{-1}$, 3 for NH_4^+ to N_2, 8 for NH_4^+ to NO_3^-, 6 for Cl^- to ClO_3^-, and 2 for Cl^- to Cl_2. The estimates shown in Figure 3.7 are based on the time when COD first declined to below 30 mg L^{-1}, a typical criteria for water reuse.[34]

The CE for COD oxidation has been known to decrease with the electrolysis time in case of direct oxidation limited by diffusion to the anode surface[29] or galvanostatic electrolysis due to a decrease in substrate concentration.[24] In our case, the differential concentrations of COD, NH_4^+, NO_3^-, and ClO_3^- are correlated with the specific passed charge (coulomb per unit volume); *i.e.*, consistent CE's with the electrolysis time. The decrease of the COD removal rate along with the [COD] was compensated by the decrease in *J*, which was proportional to $[Cl^-]$. The linear relation between the [COD] and $[Cl^-]$ also contributes to the apparent self-consistent current efficiencies.

At lower anodic potentials (L30 and L50), in which the heterogeneous RCS generation is limiting, the increase in $[Cl^-]_{ext.}$ significantly enhanced the CE. In contrast, at higher potentials, where homogeneous reactions between RCS and COD become important, the CE for COD removal was the highest in the wastewater sample H30. Oxidation of NH_4^+ to NO_3^- and N_2 were minor fractions (~ 10%) of the anodic charge transfer due to the small initial $[NH_4^+]$. The CE's for the observed residual chlorine were similar to those for ClO_3^- production and COD loss. The sum of the RCS mediated

reactions was below 40%. The loss in CE's can be attributed to O_2 evolution and RCS reduction at the cathode.

Table 3.4 summarizes the times required to reduce COD to be below 30 mg L^{-1} (t_{COD30}), as well as [COD], [NO_3^-], [ClO_3^-], [Cl_{DPD}], and corresponding specific energy consumption (SEC) for COD removal at t_{COD30}. The SEC was calculated as follows:

$$\text{Specific Energy Consumption (kWh kgCOD}^{-1}) = \frac{\int_0^t (E_a - E_C) \times I \, dt}{([COD]^0 - [COD]^t) \times V} \times 1000 \qquad (3.6)$$

where, $E_a - E_c$ and I are cell voltage (V) and current (A), $[COD]^0$ and $[COD]^t$ are COD concentration (mg L^{-1}) at the electrolysis time of zero and t (h), and V is electrolyte volume (0.06 L). For galvanostatic electrolyses, an increasing [Cl^-] decreases the SEC by decreasing the cell voltage.[13,25,27] Under potentiostatic conditions, however, the SEC

Table 3.4. Sampling time when COD below 30 mg L^{-1} was observed (t_{COD30}), concentration of COD, NO_3^-, ClO_3^- and total chlorine at t_{COD30}, and specific energy consumption (SEC) for unit COD removal at t_{COD30} under variable applied anodic potential (L: 2.2 V, H: 3.0 V NHE) and added Cl^- concentration (10, 30, 50 mM) in electrolysis experiments using domestic wastewater samples.

ID	L30	L50	H10	H30	H50
t_{COD30} (min)	> 360	240	360	120	180
[COD] (mg L^{-1})	93	13	11	19	28
[NO_3^-] (mM)	0.16	0.22	0.20	0.18	0.38
[ClO_3^-] (mM)	1.0	3.1	1.9	3.4	7.1
[Cl_{DPD}] (mM)	2.8	9.1	3.7	8.8	14.5
SEC (kWh $kgCOD^{-1}$)	232	96	209	176	320

value has been reported to increase with [Cl^-] or conductivity via an increase in J.[26] Under both electrolytic conditions, increasing the cell voltage or current density for a given electrolyte composition normally increases the SEC.[22] In this regard, H30 gave the best space-time yield and SEC for COD removal at the high E_a. However, an increase in cell voltage and J at E_a of 3.0 V NHE requires larger energy consumption compared to E_a of 2.2 V NHE. Thus, the minimal energy usage was obtained with $[Cl^-]_{ext.}$ of 50 mM at E_a of 2.2 V NHE, which corresponds to a cell voltage of about 4 V.

3.3.6. Hydrogen Production. The generation rate of total gaseous products, the H_2 volumetric fraction, and the H_2 molar flow rate increased with increasing current density (Table 3.5). The fraction of H_2 was ~ 40% in L30 and L50, and ~ 60% in higher E_a. Other gaseous products would include O_2, H_2O, N_2, and CO_2.[7] The CE and energy efficiency of H_2 generation were calculated as follows.

Table 3.5. Hydrogen evolution for a given duration (200 – 230 min) under variable applied anodic potential (L: 2.2 V, H: 3.0 V NHE) and added Cl^- concentration (10, 30, 50 mM) in electrolysis experiments using domestic wastewater samples; current density, flow rate of total gas products, volumetric fraction of hydrogen, molar flow rate of hydrogen, current efficiency, and energy efficiency for hydrogen generation.

ID	L30	L50	H10	H30	H50
Current Density (A m^{-2})	66.7	82.6	103	179	289
Total Gas Flow (mL min^{-1})	0.320	0.253	0.453	0.907	1.720
H_2 Fraction (%)	35.1	41.1	52.6	54.3	59.2
H_2 Generation Rate (μmol min^{-1})	5.02	4.64	10.7	22.0	45.4
Current Efficiency (%)	44.8	33.5	55.4	73.2	84.1
Energy Efficiency (%)	18.0	14.0	16.9	18.5	26.0

$$\text{Current Efficiency for } H_2 \text{ production (\%)} = \frac{2 \times F \times Q_{H_2} \times t}{\int I \, dt} \times 100 \quad (3.7)$$

$$\text{Energy Efficiency for } H_2 \text{ production (\%)} = \frac{3600 \times (78\ Wh\ mol^{-1}) \times Q_{H_2} \times t}{\int (E_a - E_c) \times I \, dt} \times 100 \quad (3.8)$$

where, $E_a - E_c$ and I are cell voltage (V) and current (A), Q_{H_2} is H_2 molar production rate (mol sec^{-1}), t is time for gas collection (sec), and F is Faraday constant (96485.3 C mol^{-1}). The CE for H_2 generation was below 50% at low E_a and then increased with increasing J up to 84% at higher E_a. The remaining fraction of electron transfer at the cathode can be attributed to the combined reduction of RCS and O_2.[5,8,35] In particular, a reduction of the RCS would reduce the current efficiency both for desired anodic and cathodic reactions. We previously estimated[7,8,21] the CE for hydrogen generation to be from 50% to 90% depending on cell voltage and, more importantly, the relative concentration of organic electron doners to chloride. An augmented presence of electron donors significantly increases the CE for H_2 generation via quenching the RCS. The energy efficiency for H_2 production was estimated to be from 14% to 26%. Higher energy efficiencies up to 46% have been reported under lower cell voltages (~ 3 V)[7] or under a photoelectrocatalytic operation of the BiO_x/TiO_2 anode.[10] H_2 generated as a primary by-product in WEC or PWEC can be used in either a proton exchange membrane (PEM) or solid-state fuel cell. Therefore, a moderate reduction in the SEC is expected when utilizing the produced H_2 as a back-up energy source for the PWEC.

3.3.7. Prototype (20 L) PV Powered Wastewater Electrolysis. If a PV panel DC output is connected directly to an electrolysis reactor, then the cell voltage and current will be

affected by the electrolyte conductivity, temperature, and solar intensity. The $E_a - E_c$ and J values are determined by the characteristic I–V curve of a PV panel at a given incident solar radiation, the panel temperature, and the resistance of the electrolysis cell.[36] We had previously reported[8] a solar energy conversion efficiency below 2% when using a PV panel that was directly connected to an electrolysis cell containing industrial wastewater. In order to increase the solar energy conversion efficiency, we employed a rechargeable lead acid battery regulated by a charge controller to generate an electrical energy output of ~ 84 W (12 V × 7 A), while maintaining a constant cell voltage.

For the solar roof-top experiment, 50 mM of NaCl was added to a domestic wastewater sample to maintain a cell voltage of 3.9 V on average, which was close to the operating condition of the least energy consumption in the benchtop experiments (L50). The current was 16.7 A, corresponding to a current density of 20.9 A m^{-2}. The larger-scale prototype reactor, with the PV panel as a power source, had a similar rate of COD removal with L50; for the initial [COD] of 180 mg L^{-1} was reduced to 21 mg L^{-1} after 4 h of reaction. We also confirmed that *in-situ* generation of free chlorine[18,37] leads to the disinfection of the total coliform and fecal coliform bacterial load (Figure 3.8). The initial bacterial concentration was 7.8×10^5 CFU 100 mL^{-1} for total coliforms and 8.0×10^4 CFU 100 mL^{-1} for fecal coliforms. A majority of the coliforms (50 – 80 %) were eliminated within 30 min. Complete disinfection was observed after 3 h of electrolysis along with a significant decrease in [COD].

The effluents from the scaled-up PWEC would be of sufficient water quality to be reclaimed for nonpotable purposes.[34] On the other hand, further anodic oxidation of the

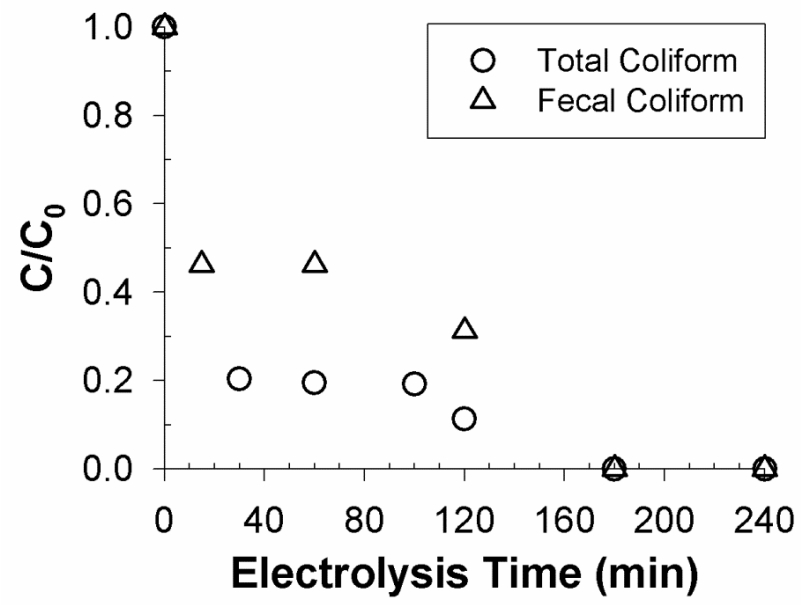

Figure 3.8. Time profiles for normalized concentration of total and fecal coliform during photovoltaic-powered wastewater electrolysis cell (PWEC, 20 L) experiment using domestic wastewater (cell voltage: 4.9 V, added Cl^- concentration: 50 mM).

RCS leads to the production of ClO_3^-, which has potential environmental health risks.[19] In the benchtop WEC (L50), the $[ClO_3^-]$ after 4 h of electrolysis was 3.0 mM. At this concentration, the reuse of the treated water would be restricted to a closed-loop recycled water system to be used for toilet flushing and for wash water. A mass balance analysis for chlorine species indicates that the sum of Cl^-, Cl_{DPD}, and ClO_3^- concentration deviate the initial chloride concentration by no more than 0.1 mM. Therefore, chlorinated byproducts other than ClO_3^- would be in a trace-level concentration.

Well-designed PWEC could be utilized within self-contained toilet facilities to provide suitable decentralized wastewater treatment systems. The energy consumption per unit volume of wastewater was estimated to be 13 Wh L^{-1} for the 20 L PWEC with a retention time of 4 h. We estimate that, for a community toilet with 30 users in a remote

rural area, the wastewater flow rate would be approximated at 120 L day^{-1}, assuming a low water usage (1.0 L d^{-1} $capita^{-1}$ for urine with 3.0 L d^{-1} $capita^{-1}$ for flushing).[12,38] With an average energy output from solar irradiation of 56 W m^{-2} over 8 h per day, the daily available solar energy is calculated to be 448 Wh day^{-1} m^{-2}. At this energy level, the total exposed surface area of polycrystalline PV panels that would be required for continuous operation of the PWEC would be virtually 3.5 m^2.

3.4. SUPPORTING INFORMATION

3.4.1. Electrochemical Methods. Before all electrochemical experiments, the electrodes were rinsed with acetone and a large amount of Milli-Q water. The electrode module was allowed to equilibrate with the electrolyte solution in an open circuit for 30 min while monitoring the open circuit potential of anode and cathode. As a routine procedure, the pH, conductivity and the ohmic resistance between anode and reference electrode (R) were measured before and after the electrochemical experiments. The pH and conductivity of the samples were monitored using a pH meter (Mettler Toledo, USA) and a portable conductivity meter (VWR International, USA). As shown in Figure 3.9, the conductivity increased while R decreased monotonically as the added chloride concentration increased. The anodic potentials were converted into NHE scale using E_a (NHE) = E_a (Ag/AgCl) + 0.197 V.

3.4.2. Prototype PV-powered Wastewater Electrolysis. The solar panel had a peak power output of 180 W with an open circuit voltage of 25.9 V, a short circuit current of 6.95 A, and an active surface area of 1.50 m^2 (0.95 m × 1.57 m), respectively. Incident solar irradiation was measured using a pyranometer (Apogee, USA) which ranged from

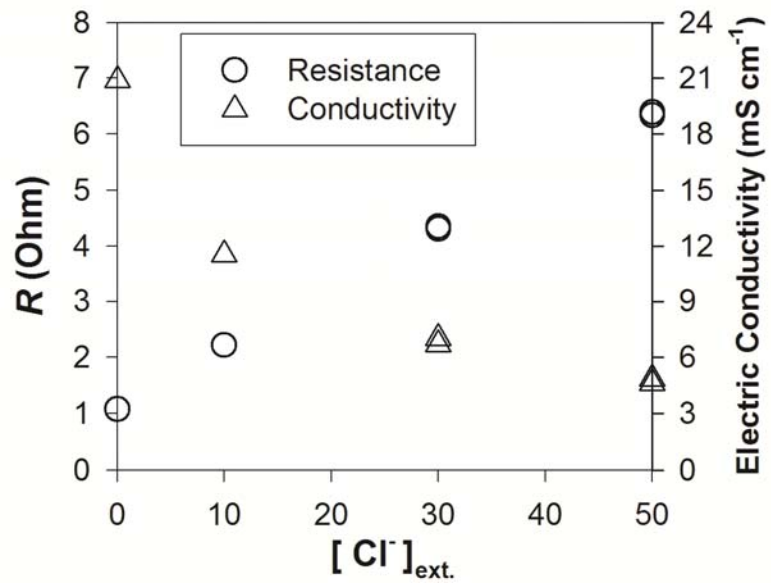

Figure 3.9. Ohmic resistance between anode and reference electrode (*R*) and electric conductivity of bulk electrolyte as functions of added Cl^- concentration ($[Cl^-]_{ext.}$) in bench-top electrolysis experiments using domestic wastewater samples.

1,000 W m^{-2} (noontime) to 600 W m^{-2} depending on the solar zenith angle. A 12 V rechargeable battery that was regulated using a charge controller was used to store excess solar energy. The voltage of the battery was controlled in order to adjust the cell voltage to be 3.9 V. The main oxidants at this cell voltage should be free chlorine species (HOCl considering the bulk pH ~ 6) since the actual anodic potential was not high enough to generate chlorine radicals. In scaling-up the WEC, an inevitable increase of ohmic voltage loss caused a reduction in current density when compared to the bench-top experiment. In these circumstances, an adjustment of electrode configuration was required to keep the free chlorine generation rate. In particular, the electrolyte volume-to-electrode surface area ratio was adjusted to 2.5 cm (20,000 cm^3 / 8,000 cm^2) while the

distance among electrodes was reduced to 2 mm, to achieve a current per unit electrolyte volume comparable with laboratory WEC (L50).

3.4.3. Analysis of Total and Fecal Coliform Concentration. In our sampling procedure, a 0.45 μm membrane filter was used to collect a microbial sample. The filter membrane is then placed on an 'mEndo' agar LES media for total coliform and an 'mFC' agar for fecal coliform for selective growth. The media plates were incubated at 35 °C for total coliform and 44.5 °C for fecal coliform for 24 h in order to promote discrete colonies. The concentration of total and fecal coliform bacteria in the wastewater was estimated in terms of CFU 100 mL^{-1} (Colony Forming Units per 100 mL).

3.5. REFERENCES

(1) *Sick Water? The central role of wastewater management in sustainable development. A rapid response assessment*; United Nations Environment Programme, UN-HABITAT, GRID-Arendal: Birkeland, 2010.; www.grida.no/publications/rr/sickwater/.

(2) Comninellis, C. Electrocatalysis in the electrochemical conversion/combustion of organic pollutants for waste-water treatment. *Electrochimica Acta* **1994,** *39* (11-12), 1857-1862.

(3) Martinez-Huitle, C. A.; Ferro, S. Electrochemical oxidation of organic pollutants for the wastewater treatment: direct and indirect processes. *Chemical Society Reviews* **2006,** *35* (12), 1324-1340.

(4) Panizza, M.; Cerisola, G. Direct And mediated anodic oxidation of organic pollutants. *Chemical Reviews* **2009,** *109* (12), 6541-6569.

(5) Park, H.; Vecitis, C. D.; Hoffmann, M. R. Electrochemical water splitting coupled with organic compound oxidation: The role of active chlorine species. *Journal of Physical Chemistry C* **2009,** *113* (18), 7935-7945.

(6) Cho, K.; Kwon, D.; Hoffmann, M. R. Electrochemical treatment of human waste coupled with molecular hydrogen production. *RSC Advances* **2014**, *4*, 4596-4608.

(7) Park, H.; Vecitis, C. D.; Hoffmann, M. R. Solar-powered electrochemical oxidation of organic compounds coupled with the cathodic production of molecular hydrogen. *Journal of Physical Chemistry A* **2008,** *112* (33), 7616-7626.

(8) Choi, J.; Qu, Y.; Hoffmann, M. R. SnO_2, IrO_2, Ta_2O_5, Bi_2O_3, and TiO_2 nanoparticle anodes: Electrochemical oxidation coupled with the cathodic reduction of water to yield molecular H_2. *Journal of Nanoparticle Research* **2012,** *14* (8).

(9) Weres, O. Electrode with surface comprising oxides of titanium and bismuth and water purification process using this electrode. U.S. Patent 7,494,583 B2, Feb. 24, 2009.

(10) Park, H.; Bak, A.; Ahn, Y. Y.; Choi, J.; Hoffmannn, M. R. Photoelectrochemical performance of multi-layered BiO_x-TiO_2/Ti electrodes for degradation of phenol and production of molecular hydrogen in water. *Journal of Hazardous Materials* **2012,** *211*, 47-54.

(11) Bard, A. J.; Faulkner, L. R., *Electrochemical methods : fundamentals and applications*. 2nd ed.; Wiley: New York, 2001.

(12) Siegrist, R.; Witt, M.; Boyle, W. C. Characteristics of rural household wastewater. *Journal of the Environmental Engineering Division-Asce* **1976,** *102* (3), 533-548.

(13) Malpass, G. R. P.; Miwa, D. W.; Mortari, D. A.; Machado, S. A. S.; Motheo, A. J. Decolorisation of real textile waste using electrochemical techniques: Effect of the chloride concentration. *Water Research* **2007,** *41* (13), 2969-2977.

(14) Shuk, P.; Wiemhofer, H. D.; Guth, U.; Gopel, W.; Greenblatt, M. Oxide ion conducting solid electrolytes based on Bi_2O_3. *Solid State Ionics* **1996,** *89* (3-4), 179-196.

(15) Trasatti, S. Progress in the understanding of the mechanism of chlorine evolution at oxide electrodes. *Electrochimica Acta* **1987,** *32* (3), 369-382.

(16) Santana, M. H. P.; De Faria, L. A. Oxygen and chlorine evolution on RuO_2+TiO_2+CeO_2+Nb_2O_5 mixed oxide electrodes. *Electrochimica Acta* **2006,** *51* (17), 3578-3585.

(17) Deborde, M.; von Gunten, U. Reactions of chlorine with inorganic and organic compounds during water treatment - Kinetics and mechanisms: A critical review. *Water Research* **2008,** *42* (1-2), 13-51.

(18) Czarnetzki, L. R.; Janssen, L. J. J. Formation of hypochlorite, chlorate and oxygen during NaCl electrolysis from alkaline-solutions at an RuO_2/TiO_2 anode. *Journal of Applied Electrochemistry* **1992,** *22* (4), 315-324.

(19) Jung, Y. J.; Baek, K. W.; Oh, B. S.; Kang, J. W. An investigation of the formation of chlorate and perchlorate during electrolysis using Pt/Ti electrodes: The effects of pH and reactive oxygen species and the results of kinetic studies. *Water Research* **2010,** *44* (18), 5345-5355.

(20) Scialdone, O.; Randazzo, S.; Galia, A.; Silvestri, G. Electrochemical oxidation of organics in water: Role of operative parameters in the absence and in the presence of NaCl. *Water Research* **2009,** *43* (8), 2260-2272.

(21) Park, H.; Choo, K.; Park, H.; Choi, J.; Hoffmann, M. R. Electrochemical oxidation and microfiltration of municipal wastewater with simultaneous hydrogen production: Influence of organic and particulate matter. *Chemical Engineering Journal* **2013,** *215-216* (15), 802-810.

(22) Fernandes, A.; Pacheco, M. J.; Ciriaco, L.; Lopes, A. Anodic oxidation of a biologically treated leachate on a boron-doped diamond anode. *Journal of Hazardous Materials* **2012,** *199*, 82-87.

(23) Miwa, D. W.; Malpass, G. R. P.; Machado, S. A. S.; Motheo, A. J. Electrochemical degradation of carbaryl on oxide electrodes. *Water Research* **2006,** *40* (17), 3281-3289.

(24) Panizza, M.; Cerisola, G. Olive mill wastewater treatment by anodic oxidation with parallel plate electrodes. *Water Research* **2006,** *40* (6), 1179-1184.

(25) Malpass, G. R. P.; Miwa, D. W.; Machado, S. A. S.; Olivi, P.; Motheo, A. J. Oxidation of the pesticide atrazine at DSA (R) electrodes. *Journal of Hazardous Materials* **2006,** *137* (1), 565-572.

(26) Gotsi, M.; Kalogerakis, N.; Psillakis, E.; Samaras, P.; Mantzavinos, D. Electrochemical oxidation of olive oil mill wastewaters. *Water Research* **2005,** *39* (17), 4177-4187.

(27) Costa, C. R.; Olivi, P. Effect of chloride concentration on the electrochemical treatment of a synthetic tannery wastewater. *Electrochimica Acta* **2009,** *54* (7), 2046-2052.

(28) Chiang, L. C.; Chang, J. E.; Wen, T. C. Indirect oxidation effect in electrochemical oxidation treatment of landfill leachate. *Water Research* **1995,** *29* (2), 671-678.

(29) Panizza, M.; Delucchi, M.; Cerisola, G. Electrochemical degradation of anionic surfactants. *Journal of Applied Electrochemistry* **2005,** *35* (4), 357-361.

(30) Szpyrkowicz, L.; Kaul, S. N.; Neti, R. N.; Satyanarayan, S. Influence of anode material on electrochemical oxidation for the treatment of tannery wastewater. *Water Research* **2005,** *39* (8), 1601-1613.

(31) Szpyrkowicz, L.; Kelsall, G. H.; Kaul, S. N.; De Favei, M. Performance of electrochemical reactor for treatment of tannery wastewaters. *Chemical Engineering Science* **2001,** *56* (4), 1579-1586.

(32) Kapalka, A.; Katsaounis, A.; Michels, N. L.; Leonidova, A.; Souentie, S.; Comninellis, C.; Udert, K. M. Ammonia oxidation to nitrogen mediated by electrogenerated active chlorine on Ti/PtO_x-IrO_2. *Electrochemistry Communications* **2010,** *12* (9), 1203-1205.

(33) Peez, G.; Saiz, J.; Ibanez, R.; Urtiaga, A. M.; Ortiz, I. Assessment of the formation of inorganic oxidation by-products during the electrocatalytic treatment of ammonium from landfill leachates. *Water Research* **2012,** *46* (8), 2579-2590.

(34) *Guidelines for water reuse*; EPA/600/R-12/618; United States Environmental Protection Agency: Washington, D.C., 2012.; nepis.epa.gov/Adobe/PDF/P100FS7K.pdf.

(35) Kim, J.; Choi, W. J. K.; Choi, J.; Hoffmann, M. R.; Park, H. Electrolysis of urea and urine for solar hydrogen. *Catalysis Today* **2013,** *199*, 2-7.

(36) Valero, D.; Ortiz, J. M.; Exposito, E.; Montiel, V.; Aldaz, A. Electrochemical wastewater treatment directly powered by photovoltaic panels: Electrooxidation of a

dye-containing wastewater. *Environmental Science & Technology* **2010,** *44* (13), 5182-5187.

(37) Bergmann, M. E. H.; Rollin, J.; Iourtchouk, T. The occurrence of perchlorate during drinking water electrolysis using BDD anodes. *Electrochim. Acta* **2009,** *54* (7), 2102-2107.

(38) *Onsite wastewater treatment systems manual*; EPA/625/R-00/008; United States Environmental Protection Agency: Washington, D.C., 2002.; nepis.epa.gov/Adobe/ PDF/P100FS7K.pdf .